



# Evaluation of site effects by developing an empirical relation between fundamental frequency and thickness of sediments for Shimla city, India

HARSH SHARMA<sup>1,\*</sup> , AMBRISH KUMAR MAHAJAN<sup>1</sup> and PRAVEEN KUMAR<sup>2</sup>

<sup>1</sup>Department of Environmental Sciences, Central University of Himachal Pradesh, Dharamshala 176 215, India.

<sup>2</sup>Department of Environment Science, Swami Vivekanand Government College, Ghumarwin 174 021, India.

\*Corresponding author. e-mail: baguharsh@gmail.com

MS received 8 August 2023; revised 11 January 2024; accepted 16 March 2024

This study focuses on developing a relation between fundamental frequency ( $f_0$ ) and the depth of sediments above the bedrock. The fundamental frequency of the site ranges from 1.25 to 27.19 Hz, whereas the depth of sediments above the bedrock varies from 2 to 145 m. The eastern Shimla region has a fundamental frequency variation from 3.6 to 5.5 Hz, whereas the western and central parts have a fundamental frequency variation from 1.24 to 5.5 Hz and high frequency ( $>20$  Hz) at isolated locations. The seismic data has also been recorded in active mode using MSOR (multichannel simulation with one receiver) to derive the dispersion curve, enabling the derivation of a 1-D, shear wave velocity ( $V_s$ ) model using a joint fit modelling procedure. The 1-D profile shows variation in  $V_s$  from 180 m/s at the top to 760 m/s at bedrock. As per the National Earthquake Hazards Reduction Program (NEHRP) classification, the sites show that almost 40% of the city area fall under stiff soil and 60% fall under very stiff soil categories. Since most of the study region is covered with forest and sloping terrain, an empirical relationship ( $H = 154.36f_0^{-1.451}$ ;  $R^2 = 0.91$ ) has been established for assessing the thickness of unconsolidated sediments. Furthermore, the thickness of sediments is determined by forward modelling by keeping the constant velocity at bedrock ( $V_b$ ) 800 m/s. Additionally, the spatial map for sediment thickness is generated using the interpolation approach in combination with the forward modelling and regression analysis techniques. The derived relationship will provide major input for the area sharing similar geographical variability, where long active seismic profiles are not possible.

**Keywords.** Forward modelling; standard penetration test; northwest Himalaya; horizontal to vertical spectral ratio.

## 1. Introduction

The northwest Himalaya, which stretches from Kashmir syntax to Garhwal Himalaya, is seismically very active and has the potential to generate major and strong earthquakes similar to those that have occurred in the past 250 years. Various

seismic hazard analyses conducted by different authors over the last three decades predict that peak ground acceleration (PGA) in the study area is expected to range from 0.12 to 0.15 g, with a 10% probability of exceeding this level in the next 50 years (Patil *et al.* 2014; Muthuganeisan and Raghukanth 2016; Sreejaya *et al.* 2022). The region

Supplementary Materials pertaining to this article is available on the *Journal of Earth System Science* website ([http://www.ias.ac.in/Journals/Journal\\_of\\_Earth\\_System\\_Science](http://www.ias.ac.in/Journals/Journal_of_Earth_System_Science)).

Published online: 13 July 2024

experienced major earthquakes in the past, such as the 1905 Kangra earthquake and a strong earthquake known as the Kinnaur earthquake in 1975, which caused significant damage to buildings and resulted in over 20,000 deaths during the 1905 Kangra earthquake. Further, the paleo-seismological investigations and seismic hazard studies indicate a potential occurrence of great earthquakes in the near future (Bilham *et al.* 1998; Kumar *et al.* 2006; Schiffman *et al.* 2013).

Numerous areas in the northwest Himalayas have also been designated as seismic gap regions by various authors (Khatri and Tyagi 1987; Rajendran and Rajendran 2005; Arora *et al.* 2012), and one such low seismicity area with a seismic gap has also been associated with the Shimla region. The Shimla region is susceptible to low-frequency waves, as the high potential seismic source zone borders the city in the east (Gharwal) and in the west (Kangra seismic source zone). The occurrence of major/great earthquakes can generate low-frequency waves from these two zones (Kumar *et al.* 2012). These waves can have disastrous effects on sites with thick, overburdened material above highly weathered metamorphic rocks. Shimla city can also be affected by the near source effect owing to internal strain as the region has not experienced any major or moderate earthquake in the last 500 years. The GPS observation for the Himalayan region also showed an alarming situation through geodetic contribution to future damaging earthquakes (Bilham and Ambraseys 2005).

Site characterization is essential to understand site behaviour during strong motion excitation. It is a key component in determining basin characteristics for risk assessment and hazard mapping. The importance of local geology and the thickness of sediments is reflected by observing the damage distribution pattern during past earthquakes such as the 1905 Kangra earthquake and the 2001 Bhuj earthquake (Middlemiss 1910; Schweig *et al.* 2003). The input parameters for site characterization are indicated by the shear wave velocity ( $V_s$ ), density and thickness of sediments. The local geological characteristics also have a significant impact on the amplification of seismic waves. According to Kramer and Steven (1996), strong ground motion will show different responses at different sites as per near-surface material properties and stiffness parameters. Therefore, delineating the sediment thickness above bedrock plays a crucial role in influencing ground motion characteristics (Nakamura 1989; Nagamani *et al.* 2020; Nath *et al.* 2022).

Over the past 20 years, numerous research studies estimated the engineering bedrock and input parameters for site response analysis (Mahajan *et al.* 2021; Nath *et al.* 2022). These studies mainly recorded the ambient noise to delineate seismic input parameters such as fundamental frequency ( $f_0$ ) and amplification ( $A_0$ ) from horizontal-to-vertical-spectral ratio (HVSR) analysis of ambient noise measurement. The HVSR technique was also utilized successfully in the geologically complex urban environment of the Indian Himalayan Region (IHR) (Paudyal *et al.* 2012; Kumar *et al.* 2023). Most researchers used the fundamental frequency with borehole records for comparison (Eisner *et al.* 2010; Trevisani and Boaga 2018). Recent studies conducted by Kumar and Mahajan (2020) also utilized the MSOR (multichannel simulation with one receiver) based inverse modelling procedure to delineate depth of the bedrock using regression analysis. The present study also aimed to access the bedrock depth with an inverse modelling procedure for Shimla city, located in the geologically complex environment, NW Himalaya, India. This study aims to search the potential of the forward modelling procedure by constraining the initial value of the  $V_s$  to best fit the synthetic curve with the experimental HVSR curve.

The study area consists of extensively metamorphic worn rocks, primarily composed of pebbles and gravels that are not suited for carrying out normal standard penetration test. Hence, it can give erroneous results. Out of all the locations where the standard penetration test (SPT) was conducted, only five provided  $N$  values up to a depth of 6 m. For the rest of the samples,  $N$  values were rejected as they exceeded 50, which negatively impacted the correlation ( $R^2 = 0.55$ ) between shear wave velocity and corrected value of standard penetration number ( $N_c$ ). To address this issue, a comprehensive site characterization study of Shimla city was planned by incorporating a blend of active and passive seismic data collection methods. The active recording involves capturing seismic data using the MSOR technique, while the passive mode records ground vibrations such as microseisms and microtremors. The primary goal of this research is to investigate the natural frequency, amplification, sediment depth, and shear wave velocity ( $V_s$ ) by utilizing a combination of active and passive geophysical methods. This technique is commonly used in the northwest Himalayas for site characterization in various urban centres (Mahajan *et al.* 2012, 2022, 2024).

The fundamental frequency and amplification for the entire city are determined by passive seismic noise measurements using the HVSR method (Nakamura 1989), while the depth of sediments and Vs are determined by MASW (multichannel analysis of surface waves) and MSOR of some selected sites.

Considering the subsurface characteristics and lithology (development of joints, fractures and weathered material) of Shimla city, determining the thickness of sediments is crucial for understanding site response. However, conducting a microtremor survey was challenging due to forest cover and residential areas, so the current investigation has successfully encompassed all accessible areas.

A relationship between resonant frequency and sediment thickness was empirically established by employing combined joint fit modelling of the dispersion and HVSR curves. This forward modelling technique was used to estimate 1-D, Vs profiles for Shimla city. These parameters are critical for various geophysical and engineering applications, including earthquake hazard assessment, groundwater management and civil infrastructure design. Also, these techniques can help to reduce the uncertainty associated with traditional methods of sediment depth estimation, which often rely on simplified assumptions and do not account for lateral heterogeneities. Incorporating more data and using more advanced modelling techniques provide a comprehensive understanding of the subsurface structure and improve the accuracy of our estimates. In this study, approximately 110 sites were evaluated using ambient noise measurements, encompassing all available sites within the city, as shown in figure 1.

## 2. Geological features of Shimla

Medlicott (1864) described the characteristic lithological association in Shimla Group as infra-Blaini which is the part of Lesser Himalaya. Subsequently, scientists like Auden (1934), West (1939), and Pilgrim and West (1928) identified the Shimla rocks as Shimla slates. The lithological classification of the Shimla Group comprises Sanjauli, Chhaosa, Kunihar, and Basantpur Formation (Srikantia and Sharma 1971). Mandi Darla volcanic and the Shali limestone are the subsurface rocks of the Shimla Group. Moreover, Brookfield and Kumar (1985) discovered discrepancies in the

thickness of various layers, as mentioned by Srikantia and Sharma (1976), and showed the presence of Jaunsar and Blaini tillites on top of these formations. In western Himalaya, the Shimla Group is dominated by carbonates, which evolved during the Precambrian epoch (Auden 1934). The Basantpur Formation, highly developed in the underlying Chhoasa Formation, also exhibits signs of deltaic deposits. The deposition from these formations particularly the sedimentation of conglomerates and sandstones in the upper part of the Sanjauli Formation exhibited in the Shimla basin (Mukhopadhyay and Banerjee 2016). Most of the sediments are mature and contain litho-clasts typical of continental margins. Field investigations also reveal that the city's subsurface comprises a diverse range of rock types, including shale, phyllites, cross-bedded sandstone, limestone, slates, siltstone, and quartzite rocks (figure 2). The palaeo-tectonic characteristics from the upper Precambrian period have been reported from Jutogh and Jaunsar faults, which are mostly present in Shimla (Kumar and Brookfield 1987).

The study area is situated in two seismic zones, the Kangra seismic zone in the west and the Gharwal seismic zone, which exhibits many earthquakes in the past and future potential of earthquake disasters (Rajendran and Rajendran 2005; Arora *et al.* 2012; Sharma and Lindholm 2012). However, historical earthquakes in the surrounding regions, including the 1905 Kangra earthquake and more recent events such as the 1991 Uttarkashi (Mw 6.7) and 1999 Chamoli (Mw 6.5) earthquakes (Kumar and Mahajan 1994; Thakur and Kumar 1994; Rajendran *et al.* 2000; Joshi 2006), all of which had intensities greater than or equal to V, highlight the importance of identifying potential risks and hazards (Mahajan *et al.* 2010; Bungum *et al.* 2017; Ghosh 2020). Paleo-seismological studies by Thakur (2004) and Kumar *et al.* (2006) revealed that earthquakes have occurred in the northwest Himalayas along the Himalayan Frontal thrust before A.D. 1700 and as early as A.D. 1200. The epicentre of these earthquakes was located nearby to the study area. With the current palaeoseismological evidence of ruptures and the northwest Himalaya's convergence rates, which range from 10 to 16 mm/yr, the region may soon be exposed to a devastating earthquake (Malik and Nakata 2003; Thakur 2004; Kannaujia *et al.* 2022). The subsurface can have complex features that cannot be properly modelled by a simple horizontally layered model. Hence, a non-

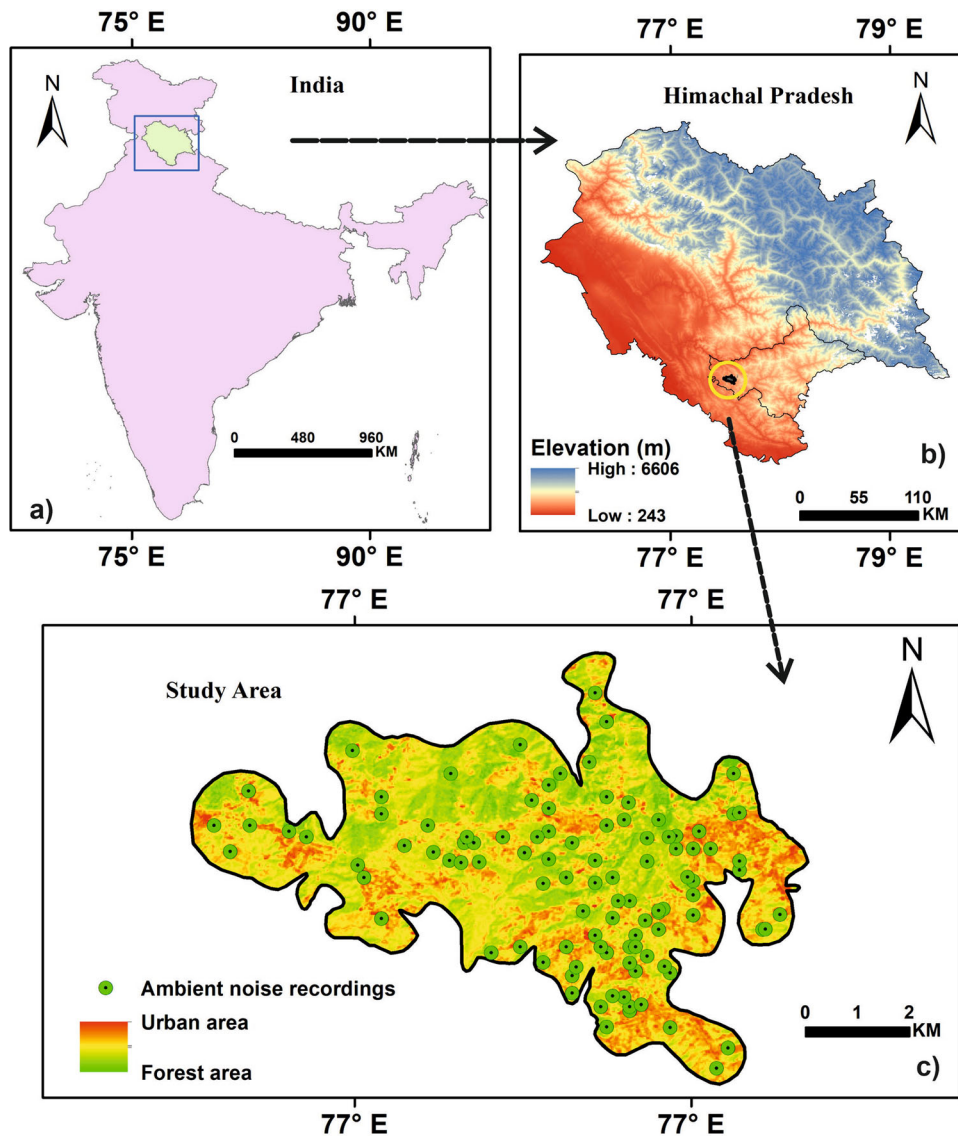


Figure 1. Location map of Shimla city for ambient noise measurements with respect to Himachal Pradesh, India.

linear correlation between frequency and depth can be used even without the measurements of ambient noise. This non-linear relationship can be utilized to infer the depth and characteristics of the underlying layer. Hence, to mitigate the risk of earthquake disasters, it is crucial to have a thorough understanding of the near-surface material's site amplification characteristics.

### 3. Methodology

The technique of recording ambient noise measurements has been used for a long time and is widely accepted and utilized as a geophysical tool. It is a non-invasive method that can quickly furnish essential insights about the seismic behaviour of a particular site. The horizontal to vertical

spectral ratio (HVSr) is used to normalize the source effect, which helps to improve the accuracy of the results Nakamura (1989, 2000). Presently, this technique is widely used worldwide as an affordable and efficient method for estimating resonance frequency ( $f_0$ ) and site amplification (A) values. It is a non-invasive geophysical technique that is available to estimate the seismic characteristics of an area while preserving high-quality data. Numerous studies have been conducted using this technique, and it has shown reliable results for a range of subsurface structures, such as geological formations and underground fractures. It has also been used for microzonation studies throughout the world, providing valuable information about the seismic behaviour of different areas (Bour *et al.* 1998; Castellaro *et al.* 2016; Mahajan *et al.* 2021, 2022). Following Nakamura

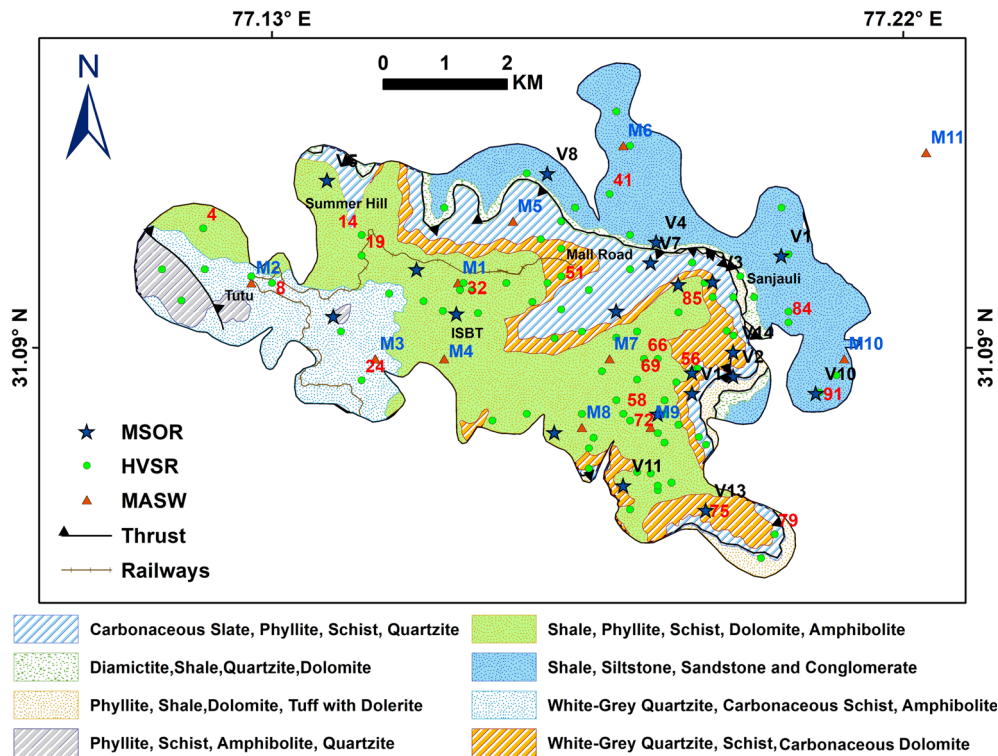


Figure 2. The geological map of Shimla city and the designated locations for conducting HVSR, MSOR, and MASW surveys.

(1989), researchers around the globe extensively tested and theoretically validated this technique worldwide in the varied geological environments for microzonation studies (Lachet and Bard 1994; Pitilakis *et al.* 1999; Mucciarelli and Gallipoli 2001; Albarello *et al.* 2011).

The Site EffectS assessments using Ambient Excitation (SESAME) guidelines, established in 2004, have been widely adopted to standardize the processing of HVSR data in geophysical studies. The HVSR method offers a significant advantage by providing information on the fundamental frequency of ground without necessitating any prior understanding of the subsurface material properties. The frequency of the HVSR peaks is generally accepted to reflect the fundamental frequency of the sediments, while the amplitude of the curve depends on the impedance contrast between the underlying bedrock and the overlying loose material. MSOR is frequently used to calculate the thickness of the sediment layers and to compare the outcomes of the HVSR and dispersion curve analyses.

### 3.1 Data acquisition and analysis

The data was gathered using the Tromino, and recordings were made by lowering the instrument

Tromino 0.05 m into a dug pit. The instrument comprises three-component orthogonal electromagnetic sensor with an embedded GPS for spatial location and a 0.1 to 1024 Hz frequency range. The sensor was levelled and perfectly coupled with the ground and was set to record a frequency of 128 Hz for 20 minutes. Grilla software was then used to analyse the recorded data from each station. The time series was divided by the software into 60 overlapping windows, each snapping 20 s, and the quietest period from the divided windows was chosen for analysis within a frequency band of 0 to 30 Hz. Triangular smoothing parameters were applied to the dataset in HVSR analysis. If there was noise in the data, it was removed, and the data was reanalysed to improve the accuracy of the HVSR curves. It is important to note that the accuracy of HVSR curves below 2 Hz can be influenced by the presence of noise (Castellaro and Mulargia 2009; Thabet 2019). Further, the analysis revealed that 90% of sites satisfied the SESAME criteria for a reliable HVSR curve, and 75% of the sites met the SESAME criteria for clear HVSR peaks, which means that HVSR obtained from the sites are of good quality. The sites which fulfil the SESAME criteria (80 sites) are used for the final analysis and preparing surface maps in the GIS platform.

### 3.2 Joint fit analysis using MSOR

Ryden *et al.* (2004) describe MSOR as a variant of the MASW method. Mahajan *et al.* (2021) reported that MSOR has been widely used in the Himalayan region. However, the depth of MSOR penetration may vary based on various factors, including lithology, the depth of the unconsolidated soil, the frequency of the geophones, and the spread. The MSOR approach outperforms the MASW method in terms of practicality, portability, cost, and speed when creating a 1-D Vs model of a near-surface material. This is because the MASW approach, unlike MSOR, requires a longer linear profile length. The results obtained from the MSOR method can be used in joint fit inversion modelling of the HVSR curve to derive a 1-D, Vs profile for a specific site. Moreover, the Tromino device, earlier used to record background noise, actively gathered seismic data with a 4.5 Hz geophone in active mode. Each geophone site has a linear array with the reception and impact source distances set at 1 and 5 m, respectively. Figure 3 provides a schematic diagram of the placement of the seismometer, geophone, and source and their incremental movement for recording multiple simulations using an active source.

To perform joint fit inversion analysis, it is necessary to utilize the base information regarding the shear wave velocity and the thickness of the topsoil. This information can be obtained using the dispersion curves derived from the MSOR technique (Ryden and Park 2006; Harutoonian *et al.* 2013; Lin and Ashlock 2016; Gupta *et al.* 2019, 2021). For inverting the HVSR curve, obtaining ambient noise measurements and shear wave velocity from the same site is necessary. In the survey, the microtremor system was placed at one end, with the geophone at a distance of 1 m and the source at 5 m from the geophone location to record the first simulation. The source and geophone (receiver) were moved systematically in increments to cover a distance of 20 to 25 m. These active simulations were used to develop a dispersion curve for each site. The data was acquired at a 1024 Hz sampling rate, activating the auxiliary channel from the Tromino layout. After recording, the data was imported using 'Grilla' software, where the dispersion curve was generated using phase and time picking. Occam's razor approach was applied during modelling to choose the maximum peaks ( $n$ ) and to produce modelled ( $n + 1$ ) layers necessary for a reliable outcome. The phase

frequency, phase velocity from the dispersion curve, and layer thickness are utilized in the inversion process of the HVSR curve. This inversion enables the determination of Vs of the top layer (Ryden *et al.* 2004; Pilz *et al.* 2010).

## 4. Results

### 4.1 HVSR

The Nakamura-based HVSR technique is based on the assumption that sediment resonance frequencies are typically lower than those of the bedrock beneath them. The depth and thickness of sedimentary layers covering the bedrock can be determined using this variation in resonance frequency (Gosar 2007; Leyton *et al.* 2013; Mahajan and Kumar 2018; Mi *et al.* 2019; Kumar and Mahajan 2020; Büyüksaraç *et al.* 2021; Molnar *et al.* 2022).

The study found that the medium frequency HVSR peaks between 3 and 10 Hz were the most prominent, although, at times, the HVSR curves became more disorderly and unpredictable towards the edges. Additionally, in some locations, the HVSR peaks indicated a significant impedance contrast (figure 4; site 75;  $f_0 = 3.66$  Hz) with clear HVSR peaks that correspond to soft material above stiff sediment or bedrock. In regions with moderate topographic relief and multiple contrasts, double HVSR peaks have been found (figure 4; site 24;  $f_0 = 1.72$  Hz). Such multiple peaks can cause unanticipated damage during a strong motion excitation. The flat curves ( $A > 2$ ) are observed in some sites with low amplitudes at variable frequency levels (figure 4; site 69;  $f_0 = 4.97$  Hz). These flat curves are a result of weak impedance contrast or the presence of weathered bedrock (phyllites, quartzite, schist, and sandstone) at the surface (Tün *et al.* 2016). Generally, a flat curve indicates a stiff soil or rock site and represents an outcrop reference site. In a few locations, the HVSR exhibits a low-frequency range of 0.32–0.9 Hz that is consistent with deep bedrock, while a nearby borehole location exhibits contrast at a shallow depth that is unrelated to the observed frequency.

### 4.2 Joint fit inversion modelling

The joint-fit modelling involves matching the synthetic HVSR with the experimental average HVSR curve (Castellaro *et al.* 2016; Gupta *et al.* 2019; Kumar and Mahajan 2020). The sediment thickness was determined for 20 sites with acquired

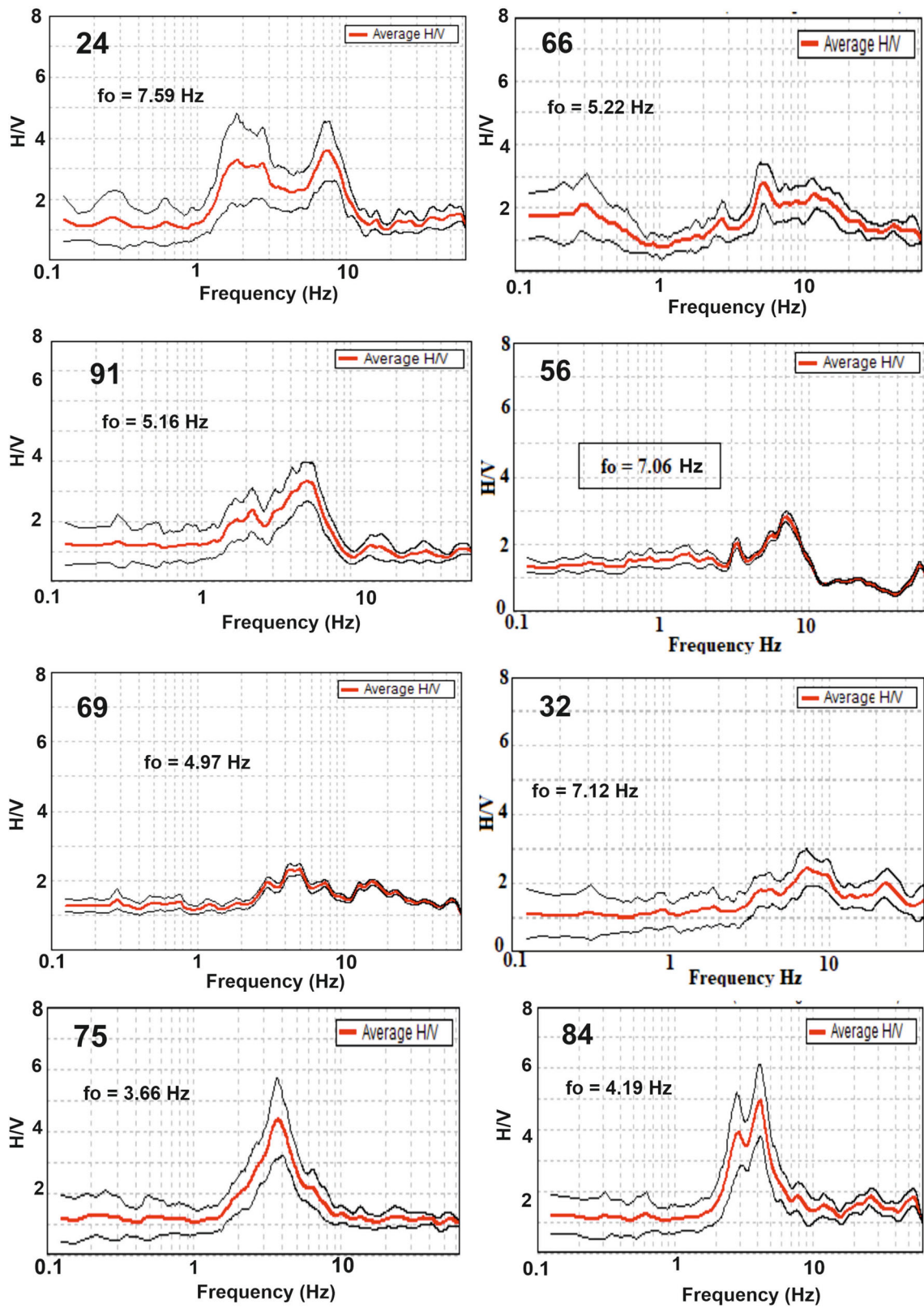


Figure 3. A few examples illustrate several instances of HVSR frequency peaks. The x-axis indicates frequency in Hz, while the y-axis represents the amplitude of the HVSR. The average HVSR plot is depicted by a prominent red line. The HVSR's 95% confidence interval is represented by two black thin lines. (i) Flat or no peak at site 69 ( $f_0 = 4.97$  Hz), (ii) multiple peaks at site 24 ( $f_0 = 7.59$  Hz and 1.87 Hz) showing the presence of multiple layers and (iii) high impedance contrast peak at site 75 ( $f_0 = 3.66$  Hz).

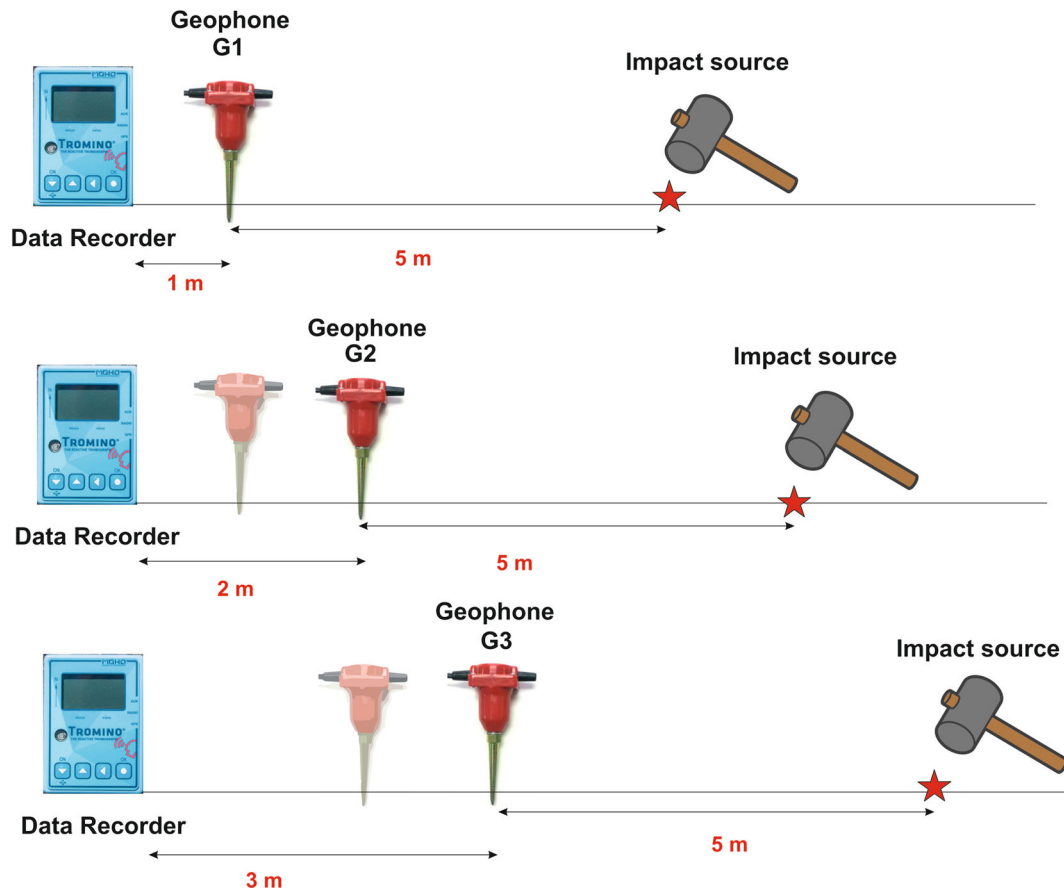


Figure 4. A schematic depiction showcasing the arrangement of the instrument (Tromino), geophone, and impact source (8 kg hammer) orientations, along with a linear profile used for data collection.

HVSR and MSOR data using a combined analysis of HVSR and dispersion curve. Figure 5 shows the observed and synthesized HVSR derived from inversion analysis. The analysis utilizes the baseline data of  $V_s$  of soil (figure 5a, b). The density and Poisson ratio are taken from the standard values for the respective soil type. The field observations, exposed sections, information on the geology, and borehole data were the primary sources of knowledge on soil type. In the dispersion curve, the fundamental mode is used to estimate deeper layers, while the higher mode is used to estimate the thickness of shallow layers, as shown in figure 5(a and b). The inversion analysis of the HVSR curves, along with joint fit modelling procedure, provides a 1-D,  $V_s$  profile (figure 5c, f, i). The result obtained for sediment thickness was then plotted against the fundamental frequency ( $f_0$ ) (figure 5). In the initial diagram (figure 5a), a frequency of 3.88 Hz corresponds to a modelled depth of 35 m with a shear wave velocity of 355 m/s on the same site.

Similarly, for the second site (V2), a frequency of 2.81 Hz aligns with a shear wave velocity of 269

m/s, indicating a depth of approximately 21 m. At the third site, a frequency of 7.25 Hz and a shear wave velocity of 397 m/s corresponds to a depth of 11 m. Analysis across 20 sites reveals that Shimla city is predominantly divided into two zones according to NEHRP classification, specifically identified as class C ( $V_s = 360\text{--}760$  m/s, very stiff soil) and D ( $V_s = 180\text{--}360$  m/s, stiff soil) classifications. These results were found to be consistent with MASW results previously performed by Muthuganesian and Raghukanth (2016).

## 5. Bedrock depth estimation with H/V forward modelling technique

In the present study, two methods are applied for estimating bedrock depth using HVSR modelling: (1) using dispersion curves derived from the MSOR technique to obtain 1-D,  $V_s$  profile (Mahajan and Kumar 2018; Gupta *et al.* 2021; Mahajan *et al.* 2022) and (2) using forward modelling procedure by keeping the bedrock velocity constant and adjusting or matching the amplitude of modelled



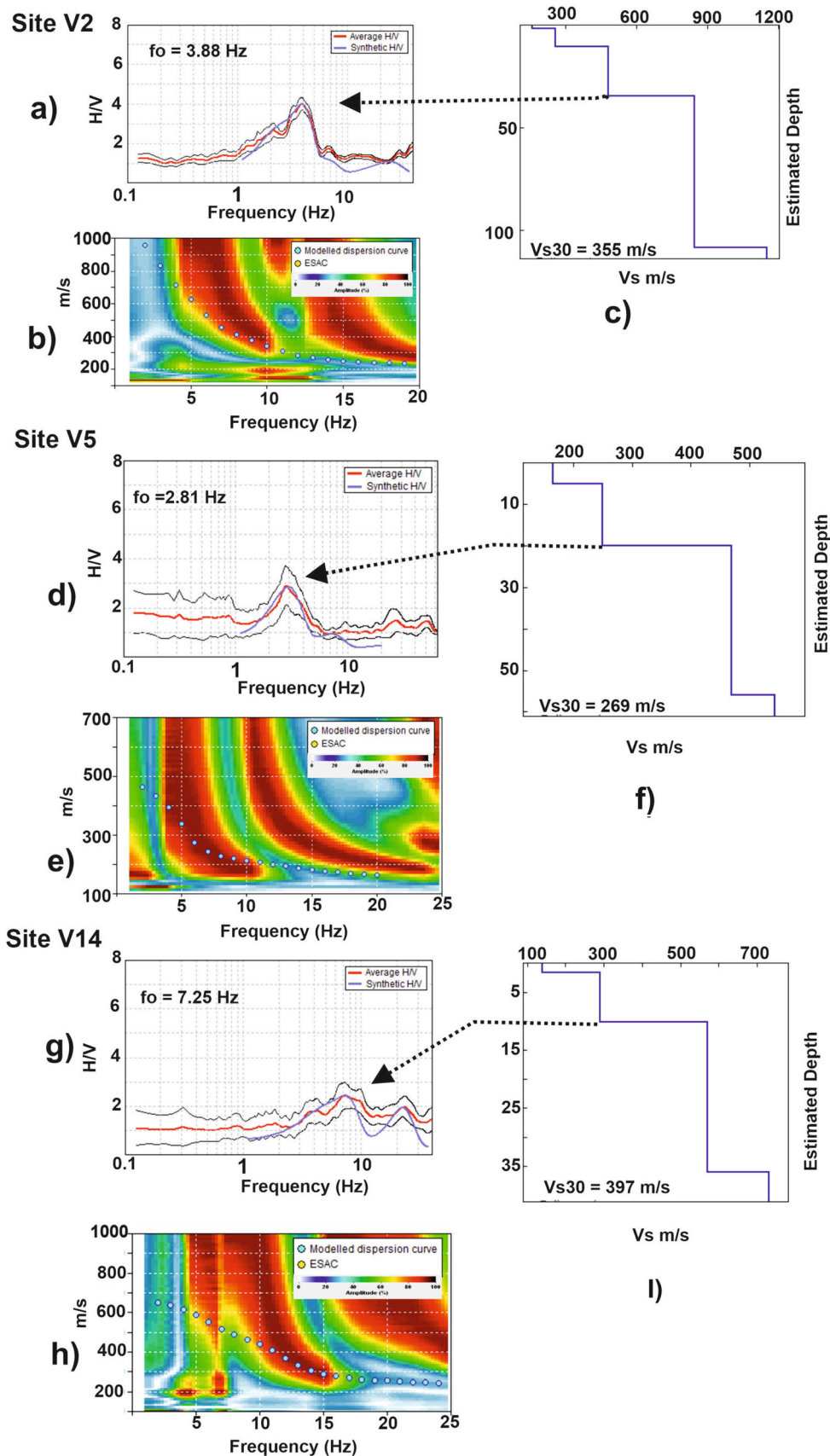


Figure 5. Outcome of the joint fit inversion modelling, with modelled HVSR curves (a, d, g), dispersion curves (b, e, h) and corresponding 1-D shear wave velocity profiles (c, f, i).

HVSR curve with observed HVSR curve (Nelson and McBride 2019). The H/V forward modelling routine is commonly used to interpolate the depth of sediments above bedrock, with the option of keeping the bedrock velocity constant or setting a specific average velocity value (ideally by MASW or any other method) for the sediment profile and varying it until the HVSR peak amplitudes match the bedrock velocity. The threshold velocity value for rock sites varies in different studies, with values ranging from 500 to 800 m/s (Yaede *et al.* 2015; Nelson and McBride 2019). The categorization of sites follows Pitilakis *et al.* (2013, 2019) site classification method. This involves grouping sites according to their geotechnical features, such as soil and rock type, depth to bedrock, and shear wave velocity with the bedrock velocity of 800 m/s.

The first stage in forward modelling processing is to identify a clear peak on the H/V spectral curve that corresponds to the fundamental mode. Initial limits for soil layer properties, such as  $V_s$ , density, thickness and Poisson's ratio, are imposed on each layer when this peak is identified. These initial constraints serve as a starting point for the parameter estimation process and can be refined as the analysis proceeds. It is common to use  $N + 1$  discrete layers in modelling when more clear peaks are present. Adjusting the  $V_s$  value can help to match the synthetic amplitude with the observed peak, with an increase in  $V_s$  leading to a decrease in the theoretical peak and a decrease in  $V_s$  leading to an increase in the theoretical peak. It is essential to know the impedance contrast in a subsoil model from the HVSR peak amplitudes. Since determining the depth of the bedrock is the primary objective, it is advised to change the thickness and  $V_s$  values for each layer throughout each iteration to improve accuracy (Del Gaudio *et al.* 2018). It is important to ensure that the values for the Poisson ratio and density are realistic and do not change significantly. This approach has been suggested by various authors (Karray and Lefebvre 2008; Castellaro and Mulargia 2009; Greaves *et al.* 2011; Nelson and McBride 2019).

For Shimla city, Muthuganesian and Raghu-kanth (2016) investigated 10 sites in the region using the MASW technique. They provided a 1-D,  $V_s$  profile, which shows variation in  $V_s$  from 200 m/s in the topsoil to 300–550 m/s at a depth of 40 m. For the present study, the 1-D,  $V_s$  model obtained by MASW is compared with the 1-D,  $V_s$  model obtained by the forward modelling technique (figure 6). It is crucial to acknowledge that

the consistency of the results depends on several factors, including the quality of data, the modelling technique and assumptions made in the modelling process. Therefore, it is important to carefully evaluate results for both deep and shallow layers and consider any discrepancies in the context of a broader geological setting.

The shallow bedrock sites are characterized by the high-frequency HVSR peak (figure 7c;  $f_0 = 12.81$  Hz), corresponding to a sediment layer thickness of 7 m. The estimated  $V_{s30}$  values from the H/V forward modelling and the MASW are 607 m/s (figure 7d) and 524 m/s (figure 6b), respectively. While maintaining the bedrock velocity of 800 m/s, the value of shear wave velocity is over-estimated by 20%, and the results are in line with a study done by Stanko and Markušić (2020) in Croatia. A significant H/V peak suggests a substantial impedance contrast between shallow bedrock and soft layers. The forward modelling of the HVSR curve corresponds to the major contrast ( $f_0 = 5.81$  Hz) between the stiff sediment and overburden material at 17 m depth (figure 7e). While the MASW profile indicates  $V_{s30} = 354$  m/s (figure 6c), the estimated  $V_{s30}$  from the H/V modelling is 433 m/s (figure 7f). In this instance, the HVSR is within 15% of the MASW- $V_{s30}$  value difference. The 20% disparity in  $V_{s30}$  results is most likely the effect of input restrictions on the H/V forward modelling soil profile.

In deep sediments,  $f_0 = 1.69$  Hz (figure 7a), when comparing  $V_{s30} = 269$  m/s (figure 7b) from H/V modelling to  $V_{s30} = 254$  m/s from MASW (figure 6a) indicates an estimated bedrock depth of 65 m (difference less than 5%). In general, there are 10–15% differences between  $V_{s30}$  values calculated from geophysical data and those obtained from H/V forward modelling, which are correlated with the observed HVSR curve. By using a single velocity of  $V_s$  800 m/s at the bedrock, the difference in the shallower sites is large, and for deeper sites, the difference is within limits, which is 5%. The presence of complex and heterogeneous underground structures, including velocity inversions, strong impedance contrasts, and lateral and vertical variations in velocity profile, can make it challenging to accurately characterize the subsurface using geophysical methods. Additionally, near-field effects can further complicate the interpretation of seismic data, and differences between resonance frequency,  $V_{s30}$ , and sediment thickness can contribute to uncertainties in the estimated subsurface properties. Studies have all reported

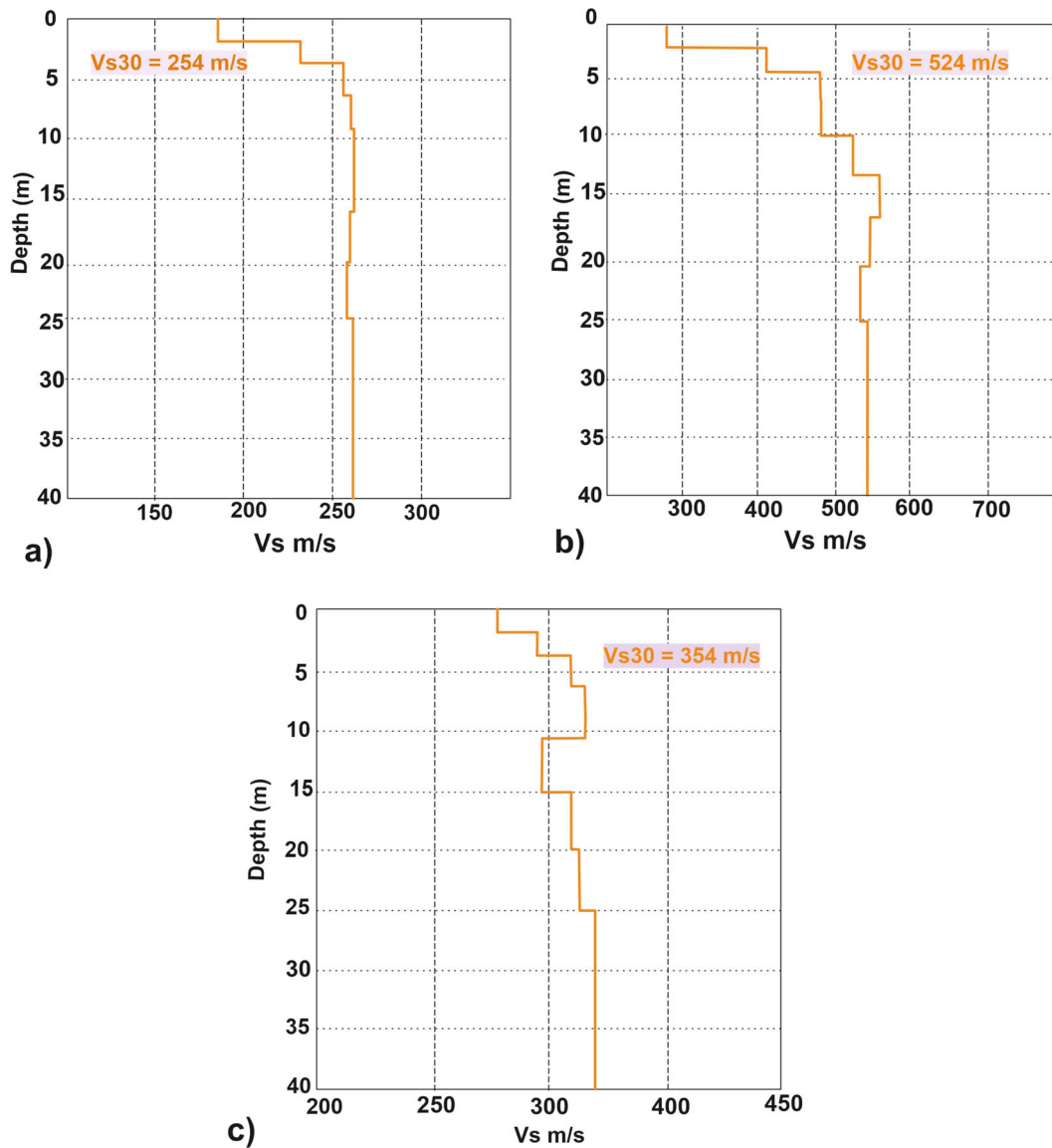


Figure 6. 1-D shear velocity profiles obtained from MASW (Muthuganesan and Raghunath 2016a). Vs values from (a) (M2) MASW Vs = 254 m/s corresponding to the site with HVSR fo = 1.69 Hz (figure 7a). (b) (M1) Vs = 524 m/s corresponding to the site with HVSR fo = 12.81 Hz (figure 7c). (c) (M6) Vs = 354 m/s corresponding to the site with HVSR fo = 5.81 Hz (figure 7e).

accuracy limitations of up to 15% when estimating subsurface properties in such complex geological settings (Martin *et al.* 2013). Therefore, it is crucial to carefully consider the limitations and potential errors inherent in any geophysical study and to use multiple methods and techniques to validate the results and improve the accuracy of the estimates.

### 6. New empirical relationships between fo and H

Researchers around the world developed resonance frequency bedrock depth equations for regional basins (table 1). These equations typically focus on

alluvial areas with significant impedance contrast between overlying soft material and underlying bedrock, which were often restricted to the frequency range of 0.2–10 Hz. However, applying this method to low impedance curves (low peak) or for sensitive sites can pose a challenge to accurately determining the bedrock depth (Nelson and McBride 2019). Shimla city is distinguished by either much forested or highly urban areas, making it challenging to locate open spaces for data collection. The city is underlain by highly pulverized fragile metamorphic rocks under such conditions where open spaces are sparse, and linear profile for MSOR and MASW is difficult. Despite the challenging conditions, it was feasible to conduct

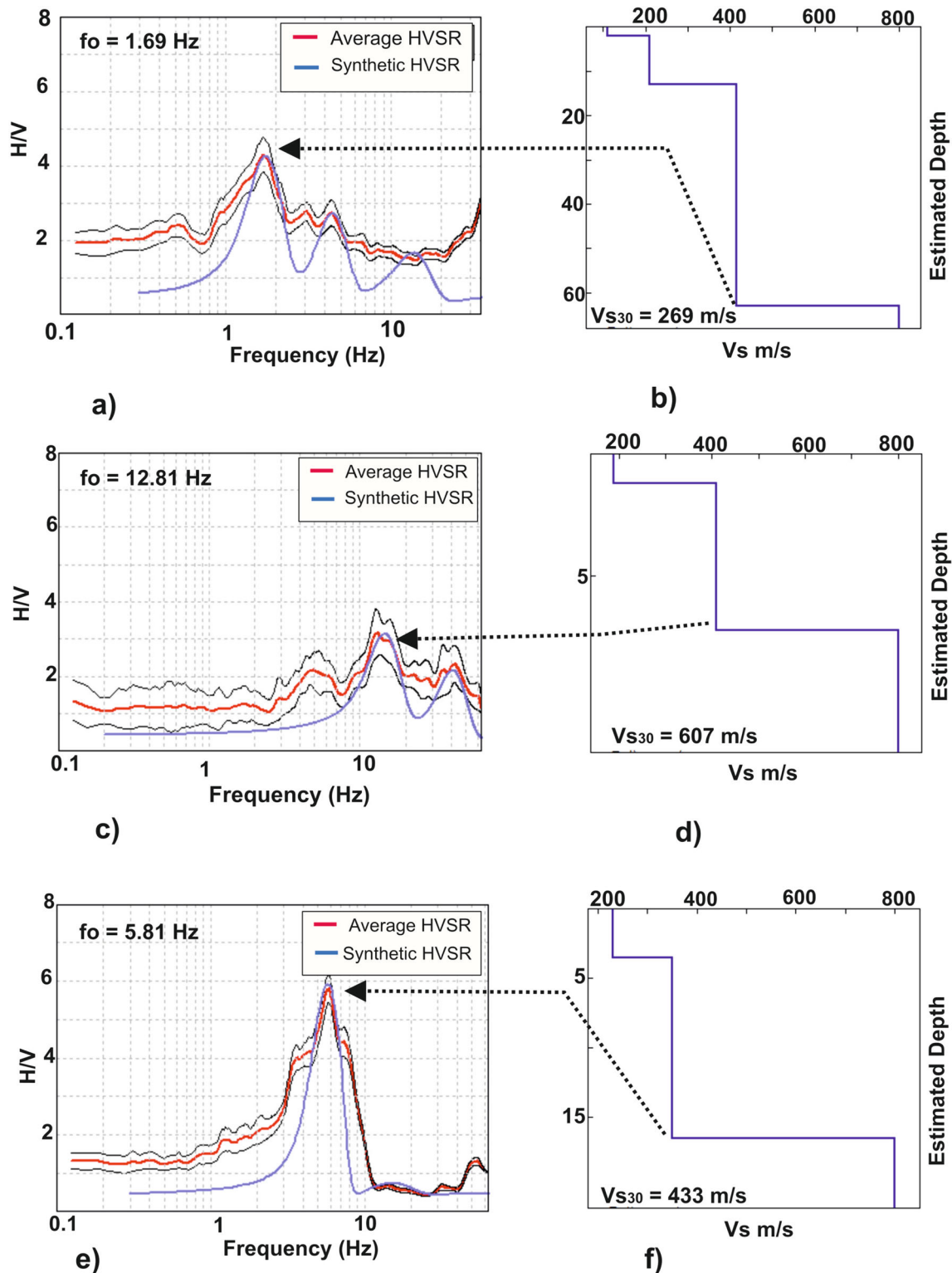


Figure 7. A few illustrations of the HVSR forward modelling technique where (a, c, e) shows the experimental HVSR with modelled HVSR whereas (b, d, f) represents the 1-D shear wave velocity profile. (i) Deep sediments with a shear wave velocity ( $V_{s30}$ ) of 269 m/s and a resonance frequency ( $f_o$ ) of 1.69 Hz. The thickness of the sediments is 62 m. (ii) Shallow bedrock with a shear wave velocity of 607 m/s and a resonance frequency of 12.81 Hz. The depth of the sediments at this site is around 7 m. (iii) A shear wave velocity of 433 m/s and a resonance frequency of 5.81 Hz. The sediments at this site have a depth of around 17 m.

ambient noise measurements to develop a correlation between the fundamental frequency and a

pseudo-depth ( $H$ ). This pseudo-depth is an estimated depth of the primary impedance contrast

Table 1. Some of the relationships between fundamental frequency and depth of sediments.

References	Region	H = afo <sup>b</sup>	
		a	b
Ibs-von Seht and Wohlenberg (1999)	Lower Rhine, West Germany	96.0	-1.388
Parolai et al. (2002)	Cologne, Germany	108.0	-1.551
Paudyal et al. (2013)	Kathmandu Valley, Nepal	146	-1.2079
Ozalaybey et al. (2011)	Izmit Bay area, Turkey	141	-1.27
Kumar and Mahajan (2020)	Kangra Valley, India	183.13	-1.542

based on empirical data (Castellaro et al. 2016; Gupta et al. 2019; Kumar and Mahajan 2020). Several researchers have previously identified various correlations between the natural frequency and pseudo-depth at various geographical places throughout the world.

Most of these equations are the result of extensive geophysical survey and their correlation with the existing borehole logs, whereas for the current Shimla city there is a sparse distribution of borehole profiles. In such limitations, Kumar and Mahajan (2020) successfully utilized a joint-fit-inversion modelling procedure to delineate the sediments thickness and Vs profile in a complex geological environment of Kangra Valley, NW Himalaya, India. The joint fit modelling employed in this study operates under the premise that the stratigraphic layers present are plane and parallel. Therefore, the existence of lateral heterogeneities within the subsurface can potentially result in erroneous conclusions being drawn from phase velocity spectra (Gupta et al. 2019). The study utilized joint-fit-inversion modelling of the dispersion and HVSR curves to determine sediment thickness. However, there are some limitations imposed by physiographic factors, and the distribution of MSOR data points was not uniform.

Nevertheless, the measurements obtained from both HVSR and MSOR at 20 selected sites were utilized in this study to develop a new correlation specific to the geographic region under investigation. This was accomplished through non-linear regression analysis to establish a correlation between sediment thickness and fundamental frequency. Figure 8 shows the pseudo depth derived from non-linear regression analysis after the joint fit modelling procedure of HVSR and MSOR seismic data recording. To get the best-fit line, the collected resonance frequency data for these 20 sites were then plotted vs. sediment thickness, which is represented by equation (1):

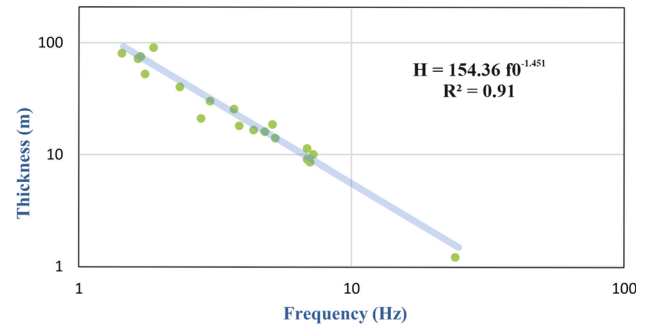


Figure 8. A non-linear regression analysis on fundamental frequency and pseudo depth of sediments derived from joint fit modelling of HVSR and dispersion curve.

$$H = 154.36f_0^{-1.451}. \tag{1}$$

The study used the MSOR and MASW methods to collect data and found a non-linear regression fit between fundamental frequency and sediment thickness. In addition, in sites where active seismic record data is not feasible, information for fundamental frequency from a passive survey can be utilized to estimate sediment thickness. The study then compared its results with other empirical relationships worldwide and found a good fit between the fundamental frequency and depth relationship and the derived regression curve, with an R<sup>2</sup> value of 0.91. The comparison of the results for the non-linear equations derived by various researchers for different regions of the world has been plotted in figure 9.

Based on shear wave velocity, Shimla city can be differentiated into three lithological types. The first type is the bedrock, which has a shear wave velocity greater than 800 m/s. The second type is fragile pulverized metamorphic soft rock, whose average shear wave velocity varies from 350 to 450 m/s. The third type is filled material, consisting mainly of gravel with some clay and silt, with an average shear wave velocity varying from 150 to

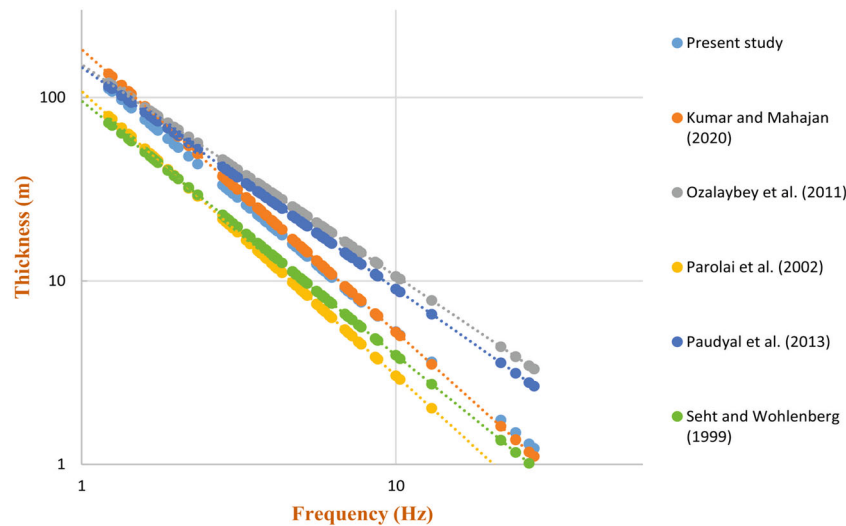


Figure 9. Various empirical relationships from around the world, including the relationship for the present study for Shimla city.

250 m/s. This non-linear equation can be used in conjunction with other geophysical techniques to validate the results. The sediment thickness determined using this method is shown in figure 10(b). It may be employed for seismic hazard analysis as well as geophysical exploration.

## 7. Discussion

Ambient noise was measured at 110 points covering an area of  $\sim 30 \text{ km}^2$  throughout Shimla city, and geophysical measurements, including MASW (Muthuganesian and Raghukanth 2016) and MSOR, were made at the same places as the free field measurements. The use of rapid passive seismic measurements provides a quick and economical way to estimate bedrock depth, which can be useful in cases where deep borehole data is not available. It is worth mentioning that modelled HVSR curve may not provide a direct proxy of subsurface condition due to lateral and geological variations or the presence of inversion at a deeper level that is not evident in HVSR curves (Xu and Wang 2021; Molnar *et al.* 2022). Therefore, it is important to interpret the results of any geophysical measurements, including ambient noise measurements, in conjunction with other geological and geotechnical data to obtain a more accurate understanding of the subsurface conditions.

The spatial map obtained from two different techniques shows differences in the sediment thickness and shear wave velocity ( $V_s$ ) (figure 10) (see Supplementary material). These differences in estimates between the two

techniques, joint fit modelling and forward modelling, are more pronounced for shallower sites than for deeper ones and could be due to differences in the constraints and assumptions used in the two techniques or errors in the input data. In the eastern part of the city, around the Tutu area, there are discrepancies in the depth estimates obtained from the two techniques. Joint fit modelling shows a shallower depth class of 20–30 m, while forward modelling estimates a deeper depth class of 30–40 m. Additionally, in some parts of the area, forward modelling estimates a depth class of 20–30 m, while joint fit modelling estimates a much shallower depth class of 1–10 m.

Similarly, in other parts of the city, there are significant differences in the depth classes obtained from the two techniques, with forward modelling showing deeper depth classes than joint fit modelling. Additionally, in some parts of the area, forward modelling estimates a depth class of 20–30 m, while joint fit modelling estimates a much shallower depth class of 1–10 m (around M3 MASW). The differences in estimates could be due to the complexity of the geology of the structure and the input constraints used in forward modelling. However, the presence of other borehole logs could be used to validate the results obtained by these techniques. Comparing the thickness obtained from forward modelling and non-linear regression modelling, it can be concluded that both techniques complement each other. The depth of sediments obtained by the two methods may differ slightly, with forward modelling overestimating the thickness of shallower sediments compared to

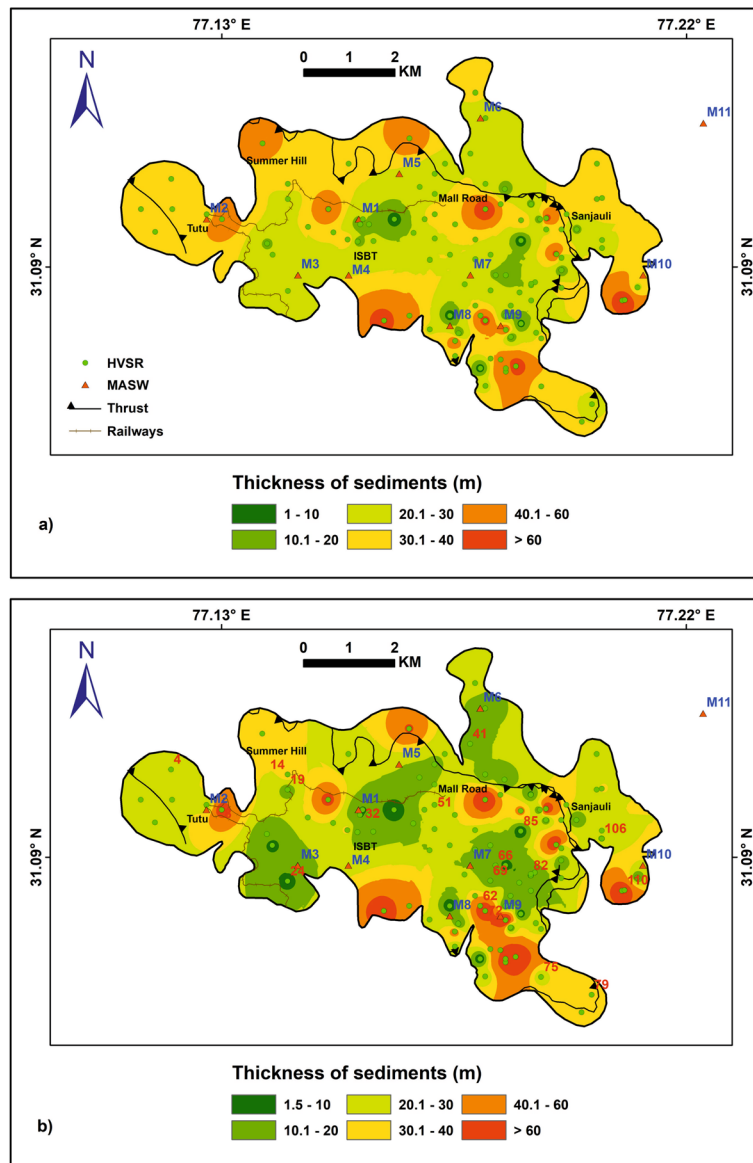


Figure 10. Map showing the depth of sediments (a) obtained from forward modelling with constant bedrock and (b) regression analysis using joint fit modelling for Shimla city.

regression modelling. The precision of estimates to drive thickness of overlying sediments can be enhanced by cross-validation using multiple geophysical techniques.

Furthermore, a non-linear regression equation has been developed to establish a relationship between SPT values and shear wave velocity ( $V_s$ ) for the Shimla city area. However, the obtained correlation coefficient ( $R^2$ ) for this relationship is only 0.554 (figure 11), which suggests that there may not be a strong correlation between the two variables. While this particular study may not have found a significant relation between standard penetration test (SPT) and shear wave velocity ( $V_s$ ), there are many other studies worldwide that

have developed empirical relationships between these ( $N_c$  and  $V_s$ ) variables for different soil types and regions (Pitilakis *et al.* 1992; Hanumantharao and Ramana 2008; Kirar *et al.* 2016). Some of these studies have found strong correlations between  $N_c$  and  $V_s$ , while others have found weaker correlations or no significant correlation at all. It is important to note that site-specific empirical relationships should be used cautiously, as they are based on a limited data set and may not apply to other sites with different soil properties or geologic conditions. It is also important to consider other factors that can affect the behaviour of soils under seismic loadings, such as soil layering, soil density and soil type. Therefore, it is recommended to use

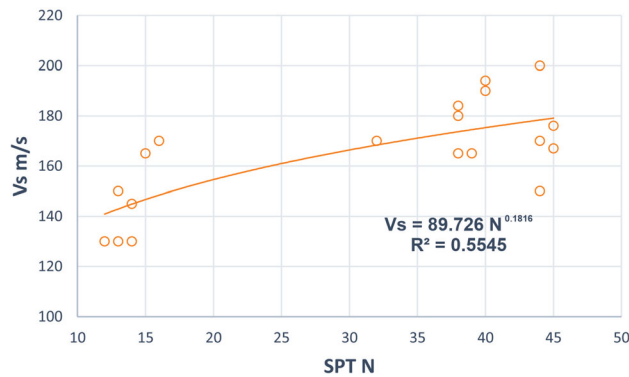


Figure 11. A non-linear regression equation between SPT (Nc) and shear wave velocity (Vs).

multiple methods and data sources to evaluate site-specific seismic hazards and soil behaviour.

## 8. Conclusion

The current study examined the relationship between the bedrock depth and fundamental frequency in Shimla city, an area in the Himalayan frontal part that has experienced unplanned modernization and is susceptible to site amplification. This study used different field measurement techniques, namely, HVSR, MSOR, and MASW, to perform H/V forward modelling and establish an empirical relationship by non-linear regression modelling. The empirical relationship derived from the study provides depth of major contrast that corresponds to the thickness of soft sediments, so the present equation also provides input for the locations in surrounding or areas sharing similar geological complexity. The advantage of using joint fit inversion and forward modelling techniques to calculate the depth of sediments is that they can provide more accurate and reliable results, especially in complex environments. Furthermore, by combining different types of data, such as HVSR and dispersion curves, these methods can account for lateral heterogeneities and other factors that may affect the interpretation of data. Additionally, the forward modelling technique allows for the testing and validation of different models and scenarios, which can help to improve the accuracy of results.

One important point highlighted in the study is that structures in Shimla city are built on fragile lithology that is extremely vulnerable to landslides. Therefore, understanding the ground response characteristics in this area is crucial for assessing the seismic hazard and developing effective

mitigation strategies. However, the standard penetration test performed on the specific site did not yield good results. This suggests that other methods, such as the ones used in this study, can be used to estimate the thickness of sediments and shear wave velocity. Overall, the study provides important insights into the ground response characteristics of Shimla city, which can be used to inform seismic hazard assessment and mitigation strategies in the area.

## Acknowledgements

The authors are extremely thankful to the authorities of the Central University of Himachal Pradesh for extending their support and facilities in various capacities. Additionally, the authors thank the Department of Industries Geological Wing and the Public Work Department of Himachal Pradesh for providing the SPT and borehole log data.

## Author statement

HS: Material preparation, data collection, analysis and drafting of original manuscript. AKM: Supervision of field survey, data interpretation and drafting of manuscript. PK: Data analysis and drafting of the revised manuscript.

## References

- Albarelo D, Cesi C, Eulilli V, Guerrini F, Lunedei E, Paolucci E, Pileggi D and Puzzilli L M 2011 The contribution of the ambient vibration prospecting in seismic microzoning: An example from the area damaged by the April 6, 2009 L'Aquila (Italy) earthquake; *Boll. Geof. Teor. Appl.* **52** 513–538.
- Arora B R, Gahalaut V K and Kumar N 2012 Structural control on along-strike variation in the seismicity of the northwest Himalaya; *J. Asian Earth Sci.* **57** 15–24, <https://doi.org/10.1016/J.JSEAES.2012.06.001>.
- Auden J B 1934 The Geology of the Krol Belt; *Rec. Geol. Surv. India* **67** 357–454.
- Bilham R and Ambraseys N 2005 Apparent Himalayan slip deficit from the summation of seismic moments for Himalayan earthquakes, 1500–2000; *Curr. Sci.* **88(10)** 1658–1663.
- Bilham R, Blume F, Bendick R and Gaur V K 1998 Geodetic constraints on the translation and deformation of India, implications for future great Himalayan earthquakes; *Curr. Sci.* **74** 213–229.
- Bour M, Fouissac D, Dominique P and Martin C 1998 On the use of microtremor recordings in seismic microzoning; *Soil Dyn. Earthq. Eng.* **17(7–8)** 465–474.



- Brookfield M and Kumar R 1985 Trace fossils from Upper Simla Group, Himachal Pradesh, India; *Bull. Indian Geol. Assoc.* **181** 25–27.
- Bungum H, Lindholm C D and Mahajan A K 2017 Earthquake recurrence in NW and central Himalaya; *J. Asian Earth Sci.* **138** 25–37.
- Büyüksaraç A, Bekler T, Demirci A and Eysisüren O 2021 New insights into the dynamic characteristics of alluvial media under the earthquake prone area: A case study for the Çanakkale city settlement (NW of Turkey); *Arab. J. Geosci.* **14** 1–15.
- Castellaro S and Mulargia F 2009 VS30 estimates using constrained H/V measurements; *Bull. Seismol. Soc. Am.* **99** 761–773, <https://doi.org/10.1785/0120080179>.
- Castellaro S, Raykova R B and Tsekov M 2016 Resonance frequencies of soil and buildings – some measurements in Sofia and its vicinity; *Natl. Congr. Phys. Sci.* 1–6.
- Del Gaudio V, Luo Y, Wang Y and Wasovski J 2018 Using ambient noise to characterise seismic slope response: The case of Qiaozhuang peri-urban hillslopes (Sichuan, China); *Eng. Geol.* **246** 374–390, <https://doi.org/10.1016/j.enggeo.2018.10.008>.
- Eisner L, Hulsey B J, Duncan P, Jurick D, Werner H and Keller W 2010 Comparison of surface and borehole locations of induced seismicity; *Geophys. Prospect.* **58**(5) 809–820.
- Ghosh U 2020 Seismic characteristics and seismic hazard assessment: Source region of the 2015 Nepal earthquake Mw 7.8 in central Himalaya; *Pure Appl. Geophys.* **177** 181–194.
- Gosar A 2007 Microtremor HVSR study for assessing site effects in the Bovec basin (NW Slovenia) related to 1998 Mw 5.6 and 2004 Mw 5.2 earthquakes; *Eng. Geol.* **91** 178–193, <https://doi.org/10.1016/j.enggeo.2007.01.008>.
- Greaves G N, Greer A L, Lakes R S and Rouxel T 2011 Poisson's ratio and modern materials; *Nat. Mater.* **10**(11) 823–837.
- Gupta R K, Agrawal M, Pal S K, Kumar R and Srivastava S 2019 Site characterization through combined analysis of seismic and electrical resistivity data at a site of Dhanbad, Jharkhand, India; *Environ. Earth Sci.* **78** 226, <https://doi.org/10.1007/s12665-019-8231-2>.
- Gupta R K, Agrawal M, Pal S K and Das M K 2021 Seismic site characterization and site response study of Nirsa (India); *Nat. Hazards* **108**(2) 2033–2057.
- Hanumantharao C and Ramana G V 2008 Dynamic soil properties for microzonation of Delhi, India; *J. Earth Syst. Sci.* **117** 719–730.
- Harutoonian P, Leo C J, Tokeshi K, Doanh T, Castellaro S, Zou J J, Liyanapathirana D S and Wong H 2013 Investigation of dynamically compacted ground by HVSR-based approach; *Soil Dyn. Earthq. Eng.* **46** 20–29.
- Ibs-von Seht M and Wohlenberg J 1999 Microtremor measurements used to map thickness of soft sediments; *Seismol. Soc. Am. Bull.* **89** 250–259, <https://doi.org/10.1785/BSSA0890010250>.
- Joshi A 2006 Analysis of strong motion data of the Uttarkashi earthquake of 20th October 1991 and the Chamoli Earthquake of 28th March 1999 for determining the Q value and source parameters; *ISSET J. Earthq. Technol.* **43**(1–2) 11–29.
- Kannaujya S, Yadav R K, Sarkar T, Sharma G, Chauhan P, Pal S K, Roy P N, Gautam P K, Taloor A K and Yadav A 2022 Unraveling seismic hazard by estimating prolonged crustal strain buildup in Kumaun-Garhwal, Northwest Himalaya using GPS measurements; *J. Asian Earth Sci.* **223** 104993.
- Karray M and Lefebvre G 2008 Significance and evaluation of Poisson's ratio in Rayleigh wave testing; *Can. Geotech. J.* **45**(5) 624–635.
- Khatti K N 1987 Great earthquakes, seismicity gaps and potential for earthquake disaster along the Himalayan plate boundary; *Tectonophys.* **138** 79–92, [https://doi.org/10.1016/0040-1951\(87\)90067-9](https://doi.org/10.1016/0040-1951(87)90067-9).
- Kirar B, Maheshwari B K and Muley P 2016 Correlation between shear wave velocity (Vs) and SPT resistance (N) for Roorkee region; *Int. J. Geosynth. Ground Eng.* **2** 1–11.
- Kramer and Steven L 1996 *Geotechnical Earthquake Engineering*; Prentice Hall, 653p.
- Kumar R and Brookfield M E 1987 Sedimentary environments of the Simla Group (Upper Precambrian), Lesser Himalaya, and their palaeotectonic significance; *Sediment. Geol.* **52** 27–43, [https://doi.org/10.1016/0037-0738\(87\)90015-7](https://doi.org/10.1016/0037-0738(87)90015-7).
- Kumar S and Mahajan A K 1994 The Uttarkashi earthquake of 20 October 1991: Field observations; *Terra Nova* **6** 95–99, <https://doi.org/10.1111/J.1365-3121.1994.TB00638.X>.
- Kumar P and Mahajan A K 2020 New empirical relationship between resonance frequency and thickness of sediment using ambient noise measurements and joint-fit-inversion of the Rayleigh wave dispersion curve for Kangra Valley (NW Himalaya), India; *Environ. Earth Sci.* **79** 256, <https://doi.org/10.1007/S12665-020-09000-8>.
- Kumar S, Wesnousky S G and Rockwell T K 2006 Paleoseismic evidence of great surface rupture earthquakes along the Indian Himalaya; *J. Geophys. Res. Solid Earth* **111** 3304, <https://doi.org/10.1029/2004JB003309>.
- Kumar N, Paul A, Mahajan A K, Yadav D K and Bora C 2012 The Mw 5.0 Kharsali, Garhwal Himalayan earthquake of 23 July 2007: Source characterization and tectonic implications; *Curr. Sci.* **102**(12) 1674–1682.
- Kumar P, Mahajan A K and Sharma M 2023 Site effect assessment and vulnerability analysis using multi-geophysical methods for Kangra city, NW Himalaya, India; *J. Earth Syst. Sci.* **132**(14) 1–13, <https://doi.org/10.1007/s12040-022-02032-7>.
- Lachet C and Bard P Y 1994 Numerical and theoretical investigations on the possibilities and limitations of Nakamura's technique; *J. Phys. Earth* **42** 377–397, <https://doi.org/10.4294/jpe1952.42.377>.
- Leyton F, Ruiz S, Sepúlveda S A, Contreras J P, Rebolledo S and Astroza M 2013 Microtremors' HVSR and its correlation with surface geology and damage observed after the 2010 Maule earthquake (Mw 8.8) at Talca and Curicó, Central Chile; *Eng. Geol.* **161** 26–33.
- Lin S and Ashlock J C 2016 Surface-wave testing of soil sites using multichannel simulation with one-receiver; *Soil Dyn. Earthq. Eng.* **87** 82–92, <https://doi.org/10.1016/J.SOILDYN.2016.04.013>.
- Mahajan A K and Kumar P 2018 Site characterisation in Kangra Valley (NW Himalaya, India) by inversion of H/V spectral ratio from ambient noise measurements and its validation by multichannel analysis of surface waves technique; *Near Surf. Geophys.* **16**(3) 314–327.

- Mahajan A K, Thakur V C, Sharma M L and Chauhan M 2010 Probabilistic seismic hazard map of NW Himalaya and its adjoining area, India; *Nat. Hazards* **53**(3) 443–457.
- Mahajan A K, Mundepi A K, Chauhan N, Jasrotia A S, Rai N and Gachhayat T K 2012 Active seismic and passive microtremor HVSR for assessing site effects in Jammu city, NW Himalaya, India – A case study; *J. Appl. Geophys.* **77** 51–62.
- Mahajan A K, Kumar P and Kumar P 2021 Near-surface seismic site characterization using Nakamura-based HVSR technique in the geological complex region of Kangra Valley, northwest Himalaya, India; *Arab. J. Geosci.* **14**(10) 826, <https://doi.org/10.1007/S12517-021-07136-W>.
- Mahajan A K, Sharma S, Patial S, Sharma H, Pandey D D and Negi S 2022 A brief address of the causal factors, mechanisms, and the effects of a major landslide in Kangra valley, North-Western Himalaya, India; *Arab. J. Geosci.* **15**(9) 925.
- Mahajan A K, Patial R, Kumar P, Sharma H, Sharma D, Kundal K and Priyanka K 2024 Site characterization of urban centers from Himalayan region using active and passive seismic methods; *Geotech. Geol. Eng.* **42** 1105–1129.
- Malik J N and Nakata T 2003 Active faults and related Late Quaternary deformation along the northwestern Himalayan Frontal Zone, India; *Ann. Geophys.* **46**(5) 917–936.
- Martin A, Stokoe K and Diehl J 2013 *ARRA-funded VS30 measurements using multi-technique approach at strong-motion stations in California and central-eastern United States* (eds Yong A *et al.*, US Department of the Interior, US Geological Survey, 59p.
- Medlicott H B 1864 On the geological structure and relations of the southern portion of the Himalayan ranges between rivers Ganges and the Ravi; *Mem. Geol. Surv. Ind.* **3**(2) 122.
- Mi B, Hu Y, Xia J and Socco L V 2019 Estimation of horizontal-to-vertical spectral ratios (ellipticity) of Rayleigh waves from multistation active-seismic records; *Geophysics* **84**(6) EN81–EN92.
- Middlemiss C S 1910 The Kangra earthquake of 4th April 1905; *Mem. Geol. Surv. India* **38** 409.
- Molnar S, Sirohey A, Assaf J, Bard P Y, Castellaro S, Cornou C, Cox B, Guillier B, Hassani B, Kawase H, Matsushima S, Sánchez-Sesma F J and Yong A 2022 A review of the microtremor horizontal-to-vertical spectral ratio (MHVSR) method; *J. Seismol.* **26**(4) 653–685.
- Mucciarelli M and Gallipoli M R 2001 A critical review of 10 years of microtremor HVSR technique; *Boll. Geofis. Teor. Appl.* **42** 255–266.
- Mukhopadhyay A and Banerjee T 2016 Stromatolites: A guideline for development of a carbonate ramp, Basantpur Formation, Neoproterozoic Simla Group in Lesser Himalaya, India; *Arab. J. Geosci.* **9** 1–18.
- Muthuganesan P and Raghukanth S T G 2016 Site-specific probabilistic seismic hazard map of Himachal Pradesh, India. Part I: Site-specific ground motion relations; *Acta Geophys.* **64** 336–361, <https://doi.org/10.1515/acgeo-2016-0010>.
- Nagamani D, Sivaram K, Rao N P and Satyanarayana H V S 2020 Ambient noise and earthquake HVSR modelling for site characterization in southern mainland, Gujarat; *J. Earth Syst. Sci.* **129** 1–14, <https://doi.org/10.1007/S12040-020-01443-8>.
- Nakamura Y 1989 A method for dynamic characteristics estimation of subsurface using microtremor on the ground surface; *Railw. Tech. Res. Inst. Q Reports* **30** 25–33.
- Nakamura Y 2000 Clear identification of fundamental idea of Nakamura's technique and its application. *Proceedings of the 12th World Conference on Earthquake Engineering*, Auckland, New Zealand, 8p.
- Nath S K, Srivastava A, Biswas A, Madan J, Ghatak C, Sengupta A and Bhaumick S 2022 Site characterization vis-à-vis probabilistic seismic hazard and disaster potential modelling in the Himalayan and sub-Himalayan tectonic ensemble from Kashmir Himalaya to northeast India at the backdrop of the updated seismic hazard of the Indian subcontinent; *Nat. Hazards Earth Syst. Sci. Discuss.* 1–43.
- Nelson S and McBride J 2019 Application of HVSR to estimating thickness of laterite weathering profiles in basalt; *Earth Surf. Process Landf.* **44** 1365–1376, <https://doi.org/10.1002/ESP.4580>.
- Ozalaybey S, Zor E, Ergintav S and Tapırdamaz M C 2011 Investigation of 3-D basin structures in the İzmit Bay area (Turkey) by single-station microtremor and gravimetric methods; *Geophys. J. Int.* **186** 883–894, <https://doi.org/10.1111/j.1365-246X.2011.05085.x>.
- Parolai S 2002 New relationships between Vs, thickness of sediments, and resonance frequency calculated by the H/V ratio of seismic noise for the Cologne area (Germany); *Bull. Seismol. Soc. Am.* **92**(6) 2521–2527, <https://doi.org/10.1785/0120010248>.
- Patil N S, Das J, Kumar A, Rout M M and Das R 2014 Probabilistic seismic hazard assessment of Himachal Pradesh and adjoining regions; *J. Earth Syst. Sci.* **123** 49–62.
- Paudyal Y R, Bhandary N P and Yatabe R 2012 Seismic microzonation of densely populated area of Kathmandu Valley of Nepal using microtremor observations; *J. Earthq. Eng.* **16**(8) 1208–1229.
- Paudyal Y R, Yatabe R, Bhandary N P and Dahal R K 2013 Basement topography of the Kathmandu Basin using microtremor observation; *J. Asian Earth Sci.* **62** 627–637, <https://doi.org/10.1016/j.jseaes.2012.11.011>.
- Pilgrim G E and West W D 1928 The structure and correlation of Simla rocks; *Mem. Geol. Surv. India* **53** 1–140.
- Pilz M, Parolai S, Picozzi M, Wang R, Leyton F, Campos J and Zschau J 2010 Shear wave velocity model of the Santiago de Chile basin derived from ambient noise measurements: A comparison of proxies for seismic site conditions and amplification; *Geophys. J. Int.* **182**(1) 355–367.
- Pitilakis K, Anastasiadis A and Raptakis D 1992 Field and laboratory determination of dynamic properties of natural soil deposits; In: *Proceedings of the 10th world conference on earthquake engineering*, Vol. 5, pp. 1275–1280.
- Pitilakis K, Raptakis D, Lontzetidis K, Tika-Vassilikou T and Jongmans D 1999 Geotechnical and geophysical description of EURO-SEISTEST, using field, laboratory tests and moderate strong motion recordings; *J. Earthq. Eng.* **3**(03) 381–409.
- Pitilakis K, Riga E and Anastasiadis A 2013 New code site classification, amplification factors and normalized response spectra based on a worldwide ground-motion database; *Bull. Earthq. Eng.* **11**(4) 925–966.

- Pitilakis K, Riga E, Anastasiadis A, Fotopoulou S and Karafagka S 2019 Towards the revision of EC8: Proposal for an alternative site classification scheme and associated intensity dependent spectral amplification factors; *Soil Dyn. Earthq. Eng.* **126** 105137.
- Rajendran C P and Rajendran K 2005 The status of central seismic gap: A perspective based on the spatial and temporal aspects of the large Himalayan earthquakes; *Tectonophysics* **395(1–2)** 19–39.
- Rajendran K, Rajendran C P, Jain S K, Murty C V R and Arlekar J N 2000 The Chamoli earthquake, Garhwal Himalaya: Field observations and implications for seismic hazard; *Curr. Sci. Bangalore* **78(1)** 45–51.
- Ryden N and Park C B 2006 Fast simulated annealing inversion of surface waves on pavement using phase-velocity spectra; *Geophysics* **71(4)** R49–R58, <https://doi.org/10.1190/12204964>.
- Ryden N, Park C B, Ulriksen P and Miller R D 2004 Multimodal approach to seismic pavement testing; *J. Geotech. Geoenviron. Eng.* **130** 636–645, [https://doi.org/10.1061/\(ASCE\)1090-0241\(2004\)130:6\(636\)](https://doi.org/10.1061/(ASCE)1090-0241(2004)130:6(636)).
- Schiffman C, Bali B S, Szeliga W and Bilham R 2013 Seismic slip deficit in the Kashmir Himalaya from GPS observations; *Geophys. Res. Lett.* **40** 5642–5645, <https://doi.org/10.1002/2013GL057700>.
- Schweig E, Gomberg J, Petersen M, Ellis M, Bodin P, Mayrose L and Rastogi B K 2003 The Mw 7.7 Bhuj earthquake: Global lessons for earthquake hazard in intraplate regions; *Geol. Soc. India* **61(3)** 277–282.
- Sharma M L and Lindholm C 2012 Earthquake hazard assessment for Dehradun, Uttarakhand, India, including a characteristic earthquake recurrence model for the Himalaya Frontal Fault (HFF); *Pure Appl. Geophys.* **169** 1601–1617.
- Sreejaya K P, Raghukanth S T G, Gupta I D, Murty C V R and Srinagesh D 2022 Seismic hazard map of India and neighbouring regions; *Soil Dyn. Earthq. Eng.* **163** 107505.
- Srikantia S V and Sharma R P 1971 Simla Group – A reclassification of the “Chail Series”, “Jaunsar Series” and “Simla Slates” in the Simla Himalaya; *Geol. Soc. India* **12** 234–240.
- Srikantia S V and Sharma R P 1976 Geology of the Shall Belt and adjoining areas; *Mem. Geol. Surv. India* **106(1)** 31–166.
- Stanko D and Markušić S, 2020 An empirical relationship between resonance frequency, bedrock depth and VS 30 for Croatia based on HVSR forward modelling; *Nat. Hazards* **103(3)** 3715–3743.
- Thabet M 2019 Site-specific relationships between bedrock depth and HVSR fundamental resonance frequency using KiK-NET data from Japan; *Pure Appl. Geophys.* **176(11)** 4809–4831.
- Thakur V C 2004 Active tectonics of Himalayan Frontal Thrust and Seismic Hazard to Ganga Plain; *Curr. Sci.* **86(11)** 1554–1560, <https://doi.org/10.1007/S12594-022-2004-3>.
- Thakur V C and Kumar S 1994 Seismotectonics of the 20 October 1991 Uttarkashi earthquake in Garhwal, Himalaya, North India; *Terra Nova* **6(1)** 90–94.
- Trevisani S and Boaga J 2018 Passive seismic prospecting in Venice historical center for impedance contrast mapping; *Environ. Earth Sci.* **77** 1–16.
- Tün M, Pekkan E, Özel O and Guney Y 2016 An investigation into the bedrock depth in the Eskisehir Quaternary Basin (Turkey) using the microtremor method; *Geophys. J. Int.* **207** 589–607, <https://doi.org/10.1093/gji/ggw294>.
- West W D 1939 The structure of the Shall Window near Simla; *Rec. Geol. Surv. India* **74(1)** 133–163.
- Xu R and Wang L 2021 The horizontal-to-vertical spectral ratio and its applications; *EURASIP J. Adv. Signal Process.* **2021** 1–10.
- Yaede J R, McBride J H, Nelson S T, Park C B, Flores J A, Turnbull S J, Tingey D G, Jacobsen R T, Dong C D and Gardner N L 2015 A geophysical strategy for measuring the thickness of the critical zone developed over basalt lavas; *Geosphere* **11(2)** 513–532, <https://doi.org/10.1130/GES01142.1>.

Springer Nature or its licensor (e.g. a society or other partner) holds exclusive rights to this article under a publishing agreement with the author(s) or other rightsholder(s); author self-archiving of the accepted manuscript version of this article is solely governed by the terms of such publishing agreement and applicable law.